doi:10.1111/j.1365-2591.2007.01256.x

Fatigue testing of a NiTi rotary instrument. Part 2: fractographic analysis

G. S. P. Cheung[1] & B. W. Darvell[2]

[1]Department of Endodontics, Faculty of Dentistry, The University of Hong Kong, Hong Kong; and [2]Dental Materials Science, Faculty of Dentistry, The University of Hong Kong, Hong Kong, China

Abstract

Cheung GSP, Darvell BW. Fatigue testing of a NiTi rotary instrument. Part 2: fractographic analysis. *International Endodontic Journal*, **40**, 619–625, 2007.

Aim To examine the topographic features of the fracture surface of a NiTi instrument after fatigue failure, and to correlate the measurements of some features with the cyclic load.

Methodology A total of 212 ProFile rotary instruments were subjected to a rotational-bending test at various curvatures until broken. The fracture surface of all fragments was examined by SEM to identify the crack origins. The crack radius, i.e. extent of the fatigue-crack growth towards the centroid of the cross-section, was also measured, and correlated with the strain amplitude for each instrument.

Results All fracture surfaces revealed the presence of one or more crack origins, a region occupied by microscopic striations, and an area with microscopic dimples. The number of specimens showing multiple crack origins was significantly greater in the group fatigued under water than in air ($P < 0.05$). A linear relationship between the reciprocal of the square root of the crack radius and the strain amplitude was discernible ($P < 0.001$), the slopes of which were not significantly different for instruments fatigued in air and water.

Conclusions The fractographic appearance of NiTi engine-files that had failed because of fatigue is typical of that for other metals. The fatigue behaviour of NiTi instruments is adversely affected by water, not only for the low-cycle fatigue life, but also the number of crack origins. There appears to be a critical extent of crack propagation for various strain amplitudes leading to final rupture (akin to the Griffith's criterion for brittle materials).

Keywords: breakage, corrosion fatigue, failure, nickel–titanium, root canal preparation, strain-life analysis.

Received 24 November 2006; accepted 19 January 2007

Introduction

Although a number of studies have attempted to examine the reasons for fracture of NiTi rotary instruments after clinical or simulated use (e.g. Sattapan *et al.* 2000, Zelada *et al.* 2002, Arens *et al.* 2003, Parashos *et al.* 2004, Schäfer & Vlassis 2004, Spanaki-Voreadi *et al.* 2006), very few have performed a systematic examination of the fracture surface to identify the mode or mechanism of fracture. Hence, their conclusions (based on the lateral-view appearance of the fractured instruments without reference to the mechanism of material failure) could be erroneous (Cheung *et al.* 2005). Some recent studies of either smooth prismatic bars (for cyclic tension) or cylindrical NiTi wires (for rotational bending) have shown that the topographical features of the fracture surface generally resembled those of other metallic materials (McKelvey & Ritchie 1999, James *et al.* 2004, Morgan *et al.* 2004).

Fatigue failure, typically, is 'brittle' macroscopically; that is, little plastic deformation (in lateral view) is discernible on either side of the fracture. The transgranular propagation, normal to the direction of maximum resolved tension, of the fatigue crack gradually reduces the intact area of the cross-section. The part then

Correspondence: Dr Gary S. P. Cheung, Floor 3A, Prince Philip Dental Hospital, 34 Hospital Road, Saiyingpun, Hong Kong, China (Tel.: +852 2859 0288; fax: +852 2559 9013; e-mail: spcheung@hku.hk).

fractures catastrophically at the 'final' load cycle that triggers a rapid and unstable growth of the fatigue crack (or so-called 'fast fracture') – the situation is analogous to a brittle material containing a flaw (or microcrack) of certain dimension and subjected to a stress of a critical magnitude, which concept is embodied in Griffith's Law (Anderson 2005). The Griffith criterion is based on the calculation of specific work (energy) of fracture. That is, crack growth will occur when the amount of energy (strain energy in an object containing a flaw) released because of advancement of the crack front is larger than the amount of energy absorbed (in the form of surface energy of two newly formed surfaces) (ASM International 1996). For brittle materials, the critical condition whereby a crack will grow spontaneously, so-called rapid or unstable crack growth, is when the fracture toughness of the material, $K_c = \sigma_c \cdot (\pi a)^{1/2}$, is exceeded (where σ_c is the critical stress, and a the crack radius; Fig. 1) (Hull 1999). As fracture toughness is a material constant, the critical stress (and hence the strain) for spontaneous crack growth is inversely proportional to the square root of the crack radius, that is, $\sigma_c \propto a^{-1/2}$. Whether NiTi rotary instruments 'obey' this rule, prior to final breakage, is unknown. On the other hand, it has been commented that NiTi alloy subjected to high alternating stresses would fail with its fracture surface showing a larger area of 'fast fracture', compared with that fatigued at low-alternating stresses (Morgan *et al.* 2004).

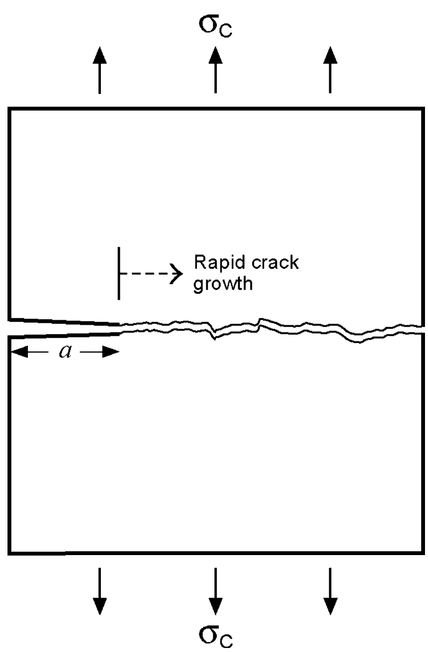

Figure 1 Schematic drawing of the condition (Griffith's criterion) whereby a crack of a certain length or radius a will propagate rapidly under the influence of a critical stress σ_c.

The vast majority of root canals are curved. An engine-file rotating in the confines of a curvature is subject to rotational bending which, indeed, is a widely-used fatigue test for structural metallic materials (Collins 1993). Part 1 of this study has reported on the strain-life relationship of a NiTi instrument subject to this mode of deformation, which results suggested that the low-cycle fatigue (LCF) life is adversely affected by water. The purposes of this present study were: (i) to describe the topographic features of the fracture surface of the instrument after fatigue failure, both in air and under water, and (ii) to examine the various features on the fracture surface, and their relationship to the cyclic load.

Materials and methods

One brand of NiTi rotary instrument (size 25, ProFile, 0.04 and 0.06 taper, Dentsply Maillefer, Ballaigues, Switzerland) was tested under rotational bending. Each rotating instrument was confined into a curvature by three smooth, stainless steel pins, as described in Part 1 (Cheung & Darvell, 2007, in press). The instrument was set to run at 250 r.p.m., either in air or under water, until it fractured. The fracture fragment was collected and mounted so that its long axis was normal to the microscope stage for fractographic examination under SEM (either a Cambridge Stereoscan 440, Cambridge, UK, or an XL-30cp, Phillips, Eindhoven, the Netherlands). A general view, usually at ×200 magnification, and high-power views of each vertex were taken for each fracture cross-section.

From the overall view, the crack initiation site(s) was identified by noting the chevron pattern, also called 'herringbone marks' (Brooks & Choudhury 2002), on the fracture surface (Fig. 2), and by referring to the high-power views where necessary. Notice that the fractographic appearance of a fatigued metallic material always progresses from the crack origin to a zone of fatigue striations (i.e. microscopic, incremental marks left by a growing fatigue crack) and, finally, a region of dimple rupture (Hull 1999). The number of crack origin(s) for each specimen was recorded, and data were examined by using the Fisher's exact test for difference between those cycled in air and under water. The region(s) in which fatigue striations could be found was outlined on the photomicrograph for each specimen. The maximum extent of the crack from the origin

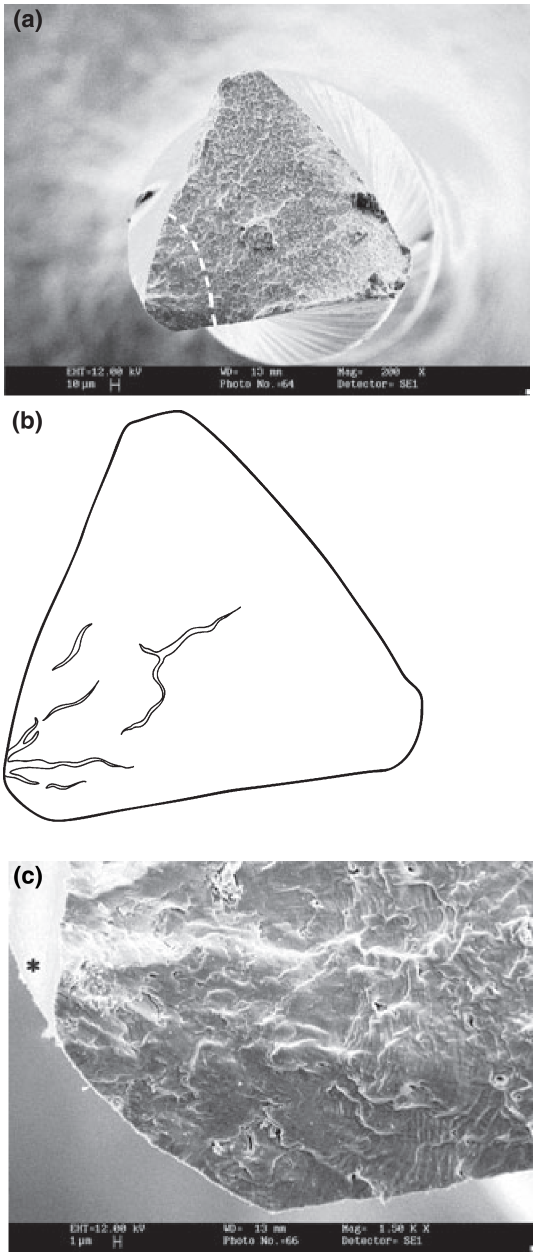

Figure 2 Fractograph of a ProFile instrument fatigued in air: (a) overall view; (b) schematic drawing of the chevron pattern in (a) pointing towards the crack origin; and (c) high-power view showing the crack origin (asterisk) and microscopic fatigue striations (right side of the field).

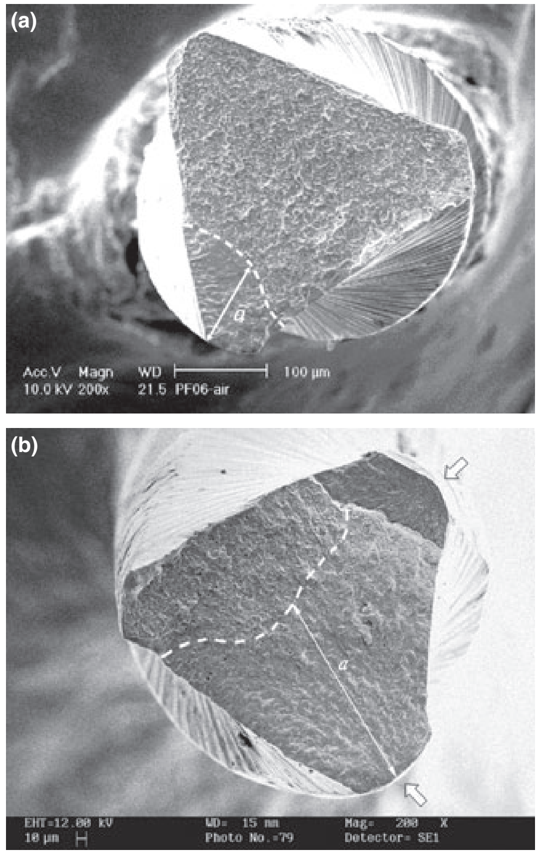

Figure 3 Photomicrograph of a fracture surface with the region of fatigue crack propagation outlined (dotted line); distance *a* was measured as the distance of 'maximum radial incursion' of the crack from the periphery towards the centroid of the cross-section: (a) with one crack origin; (b) with two crack origins (arrows).

towards the centroid of the cross-section, referred to as the 'maximum radial incursion' (MRI) below, was measured in software (IMAGEJ 1.34n, NIH, Bethesda, MD, USA) on each photomicrograph (Fig. 3). In cases where there was more than one crack origin, only the distance for the one showing the greatest incursion was measured (Fig. 3b). The reciprocal of the square root of this incursion depth, that is, equivalent to 'crack radius' (as it originated from the peripheral surface), was plotted against the surface strain amplitude ε_a for each instrument. Where a regression line could be fitted to the plot, its slope was determined. The values for the slope were examined using one-way ANOVA in software (SPSS for Windows 11.0, SPSS, Chicago, IL, USA) for difference between the two environmental conditions at $\alpha = 0.05$.

Results

For every instrument, it was possible to identify the crack origin(s) by following the chevron pattern on the

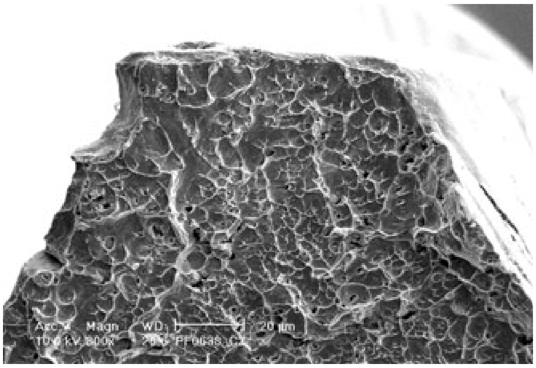

Figure 4 Fractograph of a ProFile instrument fatigued in air showing microscopic dimples involving an entire 'radial land'.

fracture surface (Fig. 2). Nearly all specimens demonstrated fatigue crack initiation at one or more cutting edge, or at the 'radial land' of the fracture cross-section. When a subsurface void or inclusion was present, it invariably was identified as the crack origin. At a short distance from the crack origin lay a region with patches of microscopic, near-parallel striation marks (Fig. 2c). An area of microscopic dimples (of various extent), which might involve the entire radial land (Fig. 4), was present on all fracture surfaces examined except for those that had been contaminated inadvertently. Some instruments, typically those rotated with a severe curvature, showed a region of crack initiation that appeared rather rough and without much in the way of identifiable features (Fig. 5). For those subjected to a lower strain amplitude, a chevron pattern was usually discernible and the extent of the crack growth region seemed to be greater than those rotated at a high strain amplitude (see Figs 3 and 5).

A single crack origin was found in approximately 90% of specimens (88/98) cycled in air, and 77% (78/101) in water; the difference was statistically significantly (Fisher's exact test, $P < 0.05$) (Table 1). A linear relationship between the reciprocal of square root of the MRI distance of the fatigue crack and the surface strain amplitude was discernible for each of the four instrument–environment combinations, with a coefficient of correlation between 0.60 and 0.77 in each case ($P < 0.001$) (Fig. 6); the slopes of the regression lines were between 1.12 (water) and 1.22 $\mu m^{-1/2}$ (air). There was no significant difference between these values (ANOVA, $P > 0.05$). The values of the x-intercept from the chart (i.e. at $\varepsilon_a = 0$, which value is equivalent to the instrument having fractured in the absence of any imposed strain) were comparable with that from calculation from raw data for each group (Table 2).

Discussion

Few studies in the past have reported on the fractographic appearance of the broken fragment obtained from clinical practice. Where available, it was limited to the demonstration of a 'typical appearance' without any systematic examination of the features for all specimens involved. In the present study, the test condition dictated that the instruments failed because of cyclic fatigue. This was confirmed by the presence of microscopic fatigue striations on all fracture surfaces, which were often located close to the crack origin and

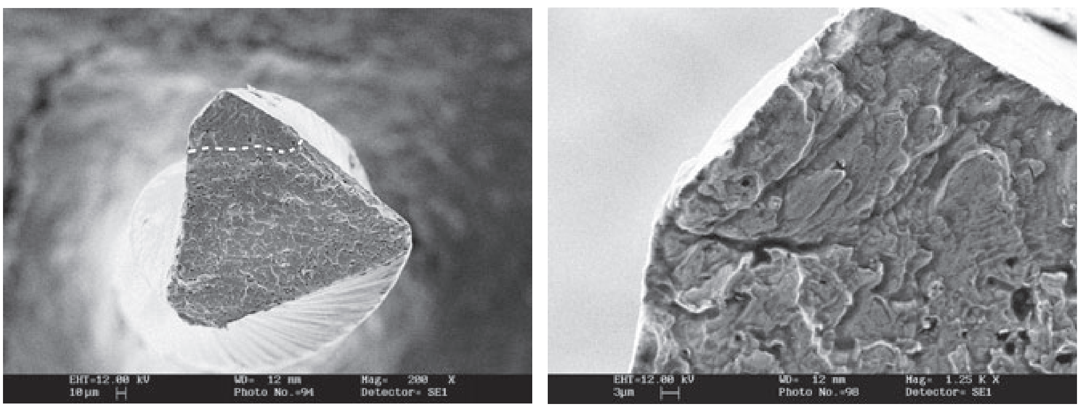

Figure 5 Fractographic appearance of the crack origin (arrow) in ProFile instruments fatigued in air at relatively high strain amplitudes ($\varepsilon_a > 2.5\%$); the steady crack-growth region outlined with a dotted line: (a) overall view; (b) high-power view of the crack origin.

Table 1 Number of crack initiation sites observed.

No. of crack origins	Number of instruments	
	In air	Under water
(a) Actual counts		
1	88	78
2	10	19
3	0	4
Subtotal	98[a]	91[b]
(b)Relative frequency of single and multiple crack origins[c]		
1	88 (90)	78 (77)
2 or more	10 (10)	23 (23)
Total	98	101

[a]Excluding three instruments that did not break when the test was abandoned, and another five that were contaminated inadvertently during processing.
[b]Excluding three that did not break when the test was abandoned, and another two with the fracture surface contaminated.
[c]Fisher's exact test for the 2×2 table (crack origin versus environment), $P = 0.0217$.

extended towards the centroid of the cross-section. Furthest away from the crack origin lay a region of 'fast fracture', where features typical of dimple rupture, or so-called ductile failure (of metals) (ASM International 1996, Hull 1999), could be observed. Contamination of the fracture surface gave rise to a surface that was covered by a dark (nonelectron conductive), featureless film.

The fractographic features of NiTi instruments fatigued under water are very similar to those in air (except for an increased incidence of multiple crack origins). Intergranular crack growth, a feature of corrosion-fatigue, was not detected probably because NiTi alloys generally showed a very good corrosion resistance in (aerated) water (Hodgson *et al.* 1990). Part 1 of this study showed an adverse effect of water on the LCF life of the one brand of instrument examined. The significantly greater number of crack origins observed here in similar instruments cycled under water indicated some effect of water on the material, probably on the crack initiation process. Although (micro)cracks might have been initiated elsewhere (i.e. not on the fracture plane, but with a resolved peak stress greater than that required for their initiation), these other cracks had failed to attain a critical size to become fatal, and hence were not observed on the fracture surface. On the other hand, the increased incidence of multiple crack origins on the fracture surface is an indicator of a higher probability of having a multitude of crack initiation sites over the

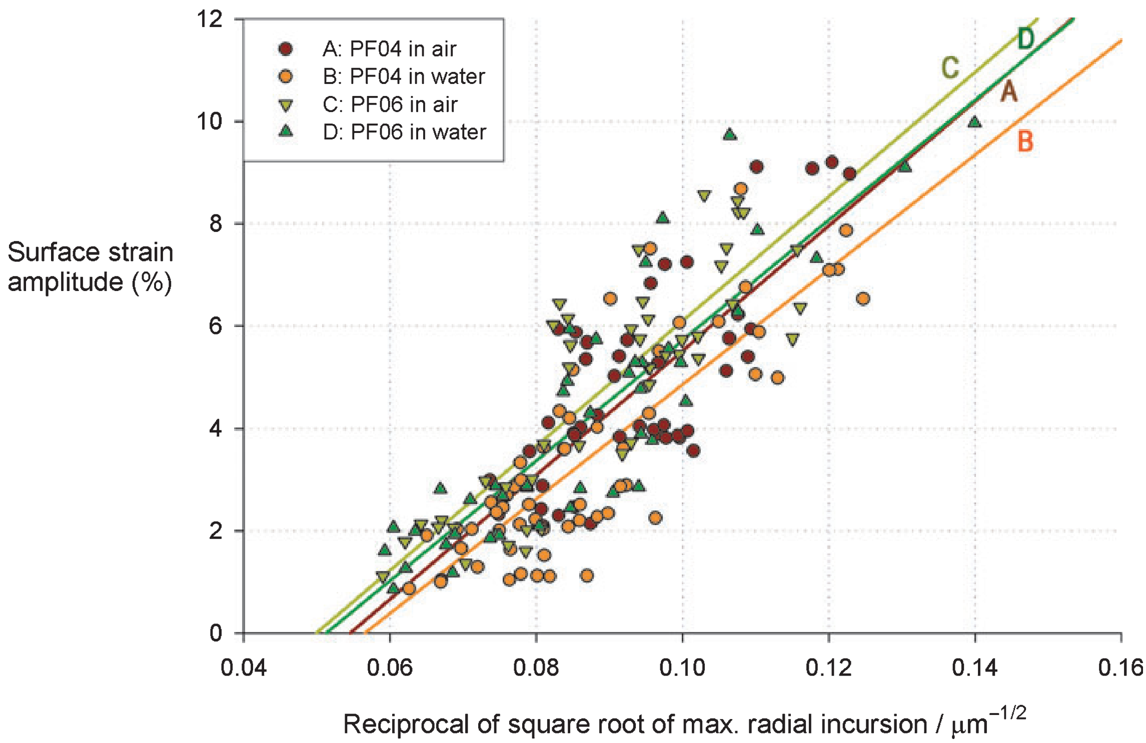

Figure 6 Relationship between the surface strain amplitude and the reciprocal of the square root of the 'maximum radial incursion' crack distance for ProFile instruments fatigued in air and under water.

Table 2 Values of calculation from raw data, and from respective regression line in the ε_a versus [maximum radial incursion (MRI) distance]$^{-1/2}$ plot.

	PF04		PF06	
	In air	In water	In air	In water
x-intercept of the regression line on ε_a versus (MRI distance)$^{-1/2}$ plot	0.055	0.057	0.50	0.051
Mean diameter of all fracture cross-sections from raw data (a)/μm	368.3	345.3	367.3	385.3
Reciprocal of square root of (a)	0.052	0.054	0.052	0.051
Calculated range (based on the 95% CI of the slope) of the value of the *x*-intercept	0.049 ~ 0.062	0.052 ~ 0.062	0.046 ~ 0.055	0.047 ~ 0.056

susceptible region for fracture (i.e. region subjected to a maximum surface strain which usually coincides with the position of maximum curvature) (Cheung 2006). Detailed, lateral-view examination of the susceptible region under high power may reveal surface defects after clinical or simulated uses (Bahia & Buono 2005, Peng *et al.* 2005), which examination is a useful adjunct to fractographic examinations.

Although not reported here, the area occupied by the steady crack-growth region, as a fraction of the total surface area of the fracture cross-section was measured for each specimen, the value of which was plotted against the strain amplitude (not shown). A significant correlation between $\log(\varepsilon_a)$ and the area fraction occupied by the steady crack-growth region was also discernible ($r^2 \approx 0.36$, $P < 0.05$), which is in keeping with the comment by Morgan *et al.* (2004). However, there was considerable scatter in such a plot (Cheung 2006) and a lack of any known, mechanical relationship between these two variables under such conditions. On the other hand, the relationship between the MRI distance and the surface strain amplitude appeared to be related to the boundary condition, as described by the Griffith criterion (for brittle materials), when the material failed.

Griffith's Law is based on the first law of thermodynamics to the effect that when a system (the cracked object in this context) goes from a nonequilibrium state (i.e. rapid crack growth) to equilibrium (part fractured and two new surfaces formed), there is a net decrease in energy (by comparing the potential energy of the cracked system and the sum of the surface energy after the fracture) (Anderson 2005). The critical stress for spontaneous crack growth (for brittle materials) is inversely proportional to the square root of the crack radius. The MRI was defined here as the maximum extension of the fatigue crack from the origin (always on the periphery) towards the centroid of the cross-section, the length of which is equivalent to the crack radius in Griffith's Law. This distance seemed to be correlated with the strain amplitude: a shorter incursion distance appeared 'enough' to lead to catastrophic failure at a higher strain amplitude. A linear relationship was discernible between ε_a and $a^{-1/2}$; that is, the NiTi instrument appears to behave like a brittle material when the fatigue strength is reached. NiTi alloys work-harden rapidly (Hodgson *et al.* 1990, Duerig & Pelton 1994). As the work-hardened NiTi instrument continues to rotate, the growing fatigue-crack (the one that first attains a critical dimension) becomes a critical flaw when the Griffith criterion is met – the material then fails in a 'brittle' manner macroscopically, although local plastic deformation (or ductile failure) is evident as microscopic dimples on the fracture surface. Such fracture is not influenced by the geometry or cross-sectional configuration of the part (see equation for fracture toughness of a material above). It can be noticed from the ε_a–$a^{-1/2}$ plot that there was an intercept on the *x*-axis, i.e. at $\varepsilon_a = 0$, the value of which is equivalent to the instrument having fractured in the absence of any imposed curvature (that is, a crack is present over the diameter of the instrument). It was found that the value of the *x*-intercept from the chart correlated well with the mean diameter of all fracture cross-sections for the corresponding group; see values in Table 2. This suggested that the NiTi instruments, under rotational bending, generally obey a Griffith-like criterion at such a boundary condition. Thus, theoretically, if one were able to determine this MRI distance, it could be feasible to predict whether an instrument (of known dimensions) may 'safely' be reused in a root canal of certain curvature where cyclic fatigue is concerned.

Conclusions

The fractographic features of NiTi rotary instruments which had failed as a result of rotational bending are typical of those of fatigue fracture of metallic materials, showing areas with steady (with microscopic fatigue striations) and rapid crack growth (dimple rupture). The LCF life of NiTi instruments subjected to rotational bending is adversely affected by water, not only for the overall fatigue life, but also the number of crack origins. The extent of the propagating fatigue crack prior to unstable, rapid growth, leading to fracture, appears to obey a Griffith-like criterion (i.e. as for brittle materials).

Acknowledgements

The authors would like to thank Mr Tony Yuen and Paul Lee of the Dental Materials Science Laboratory of the Faculty of Dentistry, HKU, for building the fatigue-testing machine; and Mr Simon Lee of the Oral Bioscience Laboratory of the Faculty of Dentistry, Ms Amy Wong of the Electron Microscope Unit, HKU, and Dr Y. Shen, Associate Professor of the Department of Operative Dentistry and Endodontics, Stomatological School and Hospital, Wuhan University, Wuhan, China for assistance with the SEMs.

References

Anderson TL (2005) *Fracture Mechanics: Fundamentals and Applications*, 3rd edn. Boca Raton, FL: CRC Press.

Arens FC, Hoen MM, Steiman HR, Dietz GC (2003) Evaluation of single-use rotary nickel–titanium instruments. *Journal of Endodontics* **29**, 664–6.

ASM International (1996) *ASM Handbook, Vol. 19: Fatigue and Fracture*. Materials Park, OH: ASM International.

Bahia MG, Buono VT (2005) Decrease in the fatigue resistance of nickel–titanium rotary instruments after clinical use in curved root canals. *Oral Surgery Oral Medicine Oral Pathology Oral Radiology and Endodontics* **100**, 249–55.

Brooks CR, Choudhury A (2002) *Failure Analysis of Engineering Materials*. New York: McGraw-Hill.

Cheung GSP (2006) *Low-Cycle Fatigue of Nickel–Titanium Rotary Root-Canal Instruments*, PhD Thesis. HKSAR, China: The University of Hong Kong.

Cheung GSP, Peng B, Bian Z, Shen Y, Darvell BW (2005) Defects in ProTaper S1 instruments after clinical use: fractographic examination. *International Endodontic Journal* **38**, 802–9.

Cheung GSP, Darvell BW (2007) Fatigue testing of a NiTi rotary instrument. Part1: strain-life relationship. *International Endodontic Journal*, in press.

Collins JA (1993) *Failure of Materials in Mechanical Design: Analysis, Prediction, Prevention*. New York, NY: John, Wiley & Sons.

Duerig TW, Pelton AR (1994) Ti-Ni shape memory alloys. In: Boyer R, Welsch G, Collings EW, eds. *Materials Properties Handbook: Titanium Alloys*. Materials Park, OH: ASM International, pp. 1035–48.

Hodgson DE, Wu MH, Biermann RJ (1990) Shape memory alloys. In: Davis JR, Allen P, Lampman SR, Zorc TB, Henry SD, Daguila JL *et al*, ed. *Metals Handbook, vol. 2: Properties and Selection: Nonferrous Alloys and Special-Purpose Materials*, 10th edn. Materials Park, OH: ASM International, pp. 897–902.

Hull D (1999) *Fractography: Observing, Measuring and Interpreting Fracture Surface Topography*. Cambridge, UK: Cambridge University Press.

James B, Murray S, Saint S (2004) Fracture characterization of Nitinol. In: Pelton AR, Duerig T, ed. *SMST-2003. Proceedings of the International Conference on Shape Memory and Superelastic Technologies*. Pacific Grove, CA: SMST Society, pp. 321–9.

McKelvey AL, Ritchie RO (1999) Fatigue-crack propagation in nitinol, a shape-memory and superelastic endovascular stent material. *Journal of Biomedical Materials Research* **47**, 301–8.

Morgan NB, Painter J, Moffat A (2004) Mean strain effects and microstructural observations during *in vitro* fatigue testing of NiTi. In: Pelton AR, Duerig T, ed. *SMST-2003. Proceedings of the International Conference on Shape Memory and Superelastic Technologies*. Pacific Grove, CA: SMST Society, pp. 303–10.

Parashos P, Gordon I, Messer HH (2004) Factors influencing defects of rotary nickel–titanium endodontic instruments after clinical use. *Journal of Endodontics* **30**, 722–5.

Peng B, Shen Y, Cheung GSP, Xia TJ (2005) Defects in ProTaper S1 instruments after clinical use: longitudinal examination. *International Endodontic Journal* **38**, 550–7.

Sattapan B, Nervo GJ, Palamara JEA, Messer HH (2000) Defects in rotary nickel–titanium files after clinical use. *Journal of Endodontics* **26**, 161–5.

Schäfer E, Vlassis M (2004) Comparative investigation of two rotary nickel–titanium instruments: ProTaper versus RaCe. Part 2. Cleaning effectiveness and shaping ability in severely curved root canals of extracted teeth. *International Endodontic Journal* **37**, 239–48.

Spanaki-Voreadi AP, Kerezoudis NP, Zinelis S (2006) Failure mechanism of ProTaper nickel–titanium rotary instruments during clinical use: fractographic analysis. *International Endodontic Journal* **39**, 171–8.

Zelada G, Varela P, Martín B, Bahíllo JG, Magán F, Ahn S (2002) The effect of rotational speed and the curvature of root canals on the breakage of rotary endodontic instruments. *Journal of Endodontics* **28**, 540–2.